Utrecht University

Institute for Theoretical Physics

Bachelor's Thesis

Water Desalination Using Capacitive Demixing

A Theoretical Analysis Of Temperature Effects

Author:
Sam Eigenhuis

Supervisors:
Prof. Dr. René van Roij
Dr. Andreas Härtel
Mathijs Janssen, MSc

"But doth suffer a sea-change
into something rich and strange"

The Tempest, Shakespeare

January 15, 2014

Abstract

At any place where a river flows into the sea, fresh and saline water are mixed. This salinity-gradient energy or "blue energy" can be harvested, e.g. using capacitive mixing. The reverse process is also possible: water desalination using capacitive demixing in a three-step cycle. In this thesis, the aim is to find the optimal desalination cycle, such that the required work per liter desalinated water is minimal. In order to find the optimal cycle, the parameter space of two variables is explored: the temperature, and the ratio between the engine volume and the water volume that is made fresh during one cycle. Numerical solutions to the lattice-gas Poisson-Boltzmann equation for parallel-plate capacitors show that desalination processes are the most efficient at low temperatures, with an increase in work of 0.31% per degree for a volume ratio of 1.33, where the needed work per secured liter fresh water $\frac{W}{V_b}$ is 1.74 kJ/liter at 0 °C. Calculations regarding the volume ratio indicate that desalination processes are the most efficient for the case when the volume of secured fresh water per cycle is large compared to the engine volume.

Contents

1 Introduction **2**
- 1.1 Blue engines . . . 2
- 1.2 Electric double-layers . . . 3
- 1.3 The reverse cycle: desalination . . . 4

2 Theory **6**
- 2.1 Debye length and Bjerrum length . . . 6
- 2.2 Dielectric constant . . . 6
- 2.3 Poisson-Boltzmann equation . . . 7
- 2.4 Lattice-gas Poisson-Boltzmann equation . . . 9
- 2.5 Work per cycle . . . 10

3 Numerical results **11**
- 3.1 Introduction . . . 11
- 3.2 Investigating the desalination cycle . . . 11
- 3.3 Temperature effects . . . 12
- 3.4 Effects of the volume ratio between the engine and the fresh water volume . . . 14

4 Conclusion and outlook **16**

5 Acknowledgements **17**

Appendix A Numerical method **19**

1 Introduction

Today's world-wide energy demand is enormous, and will only increase in the future. As the forecast of the depletion of fossil fuels like coal and oil at some point is certain, the world's attention for ways to generate power has gradually shifted to more sustainable possibilities. Nowadays, solar energy, wind energy, and energy obtained from biomass are very popular options, though many more can be named. Very recently, a way was suggested to harvest energy from CO_2 emissions [1].

A very interesting possibility in generating sustainable energy involves the use of water in some way, e.g. turbines driven by the tides [2, 3], and the mixing of fresh and salty water [4–9]. The extracting of this latter salinity-gradient energy or "blue energy", is in principle possible at any place where a river flows into the sea. Due to the irreversible mixing of fresh and salty water, the entropy of the system increases, and free energy is dissipated. This dissipation is about 2 kJ per liter of river water, which can be compared to the energy produced in a waterfall of 200 m [4].

Many existing techniques to harvest this salinity-gradient energy involve the use of membranes, like pressure-retarded osmosis [5, 6] and reverse electrodialysis [7, 8]. However, these membranes require rather advanced technology, are expensive for large-scale systems, and are easily polluted. Recently, a device was suggested by Brogioli [9] to gain this blue energy using capacitive mixing. This technique consists of a cyclic process, in which a capacitor is alternatingly charged and discharged in fresh and saline water. It is this type of engine that is the subject of this thesis.

Whereas this engine extracts energy from the mixing of fresh and saline water, it is also possible to do the reverse. In this way, energy is needed to demix saline water, such that it is possible to achieve water desalination. Of course, the need of fresh water is another important subject for some parts of the world.

In this thesis, the aim is to find the most optimal cycle, i.e. to find the cycle that requires the least input of energy per secured liter of fresh water. In order to do this, the parameter space of two variables is studied: the temperature, and the ratio between the engine volume and the water volume that is made fresh during one cycle. Desalination cycles are calculated for different temperatures and different volumes of secured fresh water per cycle. In this way, the theoretically most effective cycle for these parameters can be found. Also interesting are, amongst others, the effects of the engine size, geometry of the electrodes, and the needed input of power, i.e. required energy per unit time, but those are left for future studies.

1.1 Blue engines

The type of engine which was suggested by Brogioli, consists of a system of two porous carbon electrodes, which form a capacitor immersed in an aqueous solution, as can be seen in Fig. 1a. Having an internal surface area of the order of 10^3 m^2 per gram of carbon and a typical pore size inside the electrodes of the order of nanometers, the capacitance of these electrodes can be very large. These enormous surface areas and very small distances between the electrodes are the reason why these electrodes are sometimes called supercapacitors. The engine as proposed by Brogioli accomplishes a four-step charging and discharging cycle, as shown in Fig. 2a. First, the engine is filled with saline water and the capacitor is charged grand-canonically, i.e. in contact with a infinite large reservoir of saline water, such that the surface charge density σ on the electrodes increases. Next, the salt water in the engine is replaced with fresh water. Saline water is better able to screen the immersed surface charge than fresh water. Since the electrostatic potential depends on the ion concentration in the electrolyte, the potential across the capacitor will be lower for higher ion concentrations. As a result of the described flushing step, the electrostatic potential across the capacitor increases. The third step in the cycle consists of the discharging of the capacitor immersed in fresh water, and in the fourth step the fresh water is replaced by salt water again. Then, the system has returned to its initial state, and the cycle can be repeated. By making the salt water more fresh and the fresh water more salty, the ionic entropy of the system increases during the cycle. The cycle will effectively produce energy, because the electrodes discharge at a higher potential than at which they are charged.

By mapping this blue engine and corresponding variables to heat engines, Boon and Van Roij identified the Brogioli cycle as the "blue" equivalent of the Stirling heat engine [10]. In this mapping, the variables $\{S, T, V, -p\}$ (i.e. entropy, temperature, volume, and pressure of the gas in the Stirling engine) correspond to $\{N, \mu, Q, \Psi\}$ (i.e. number of salt ions, their chemical potential, the charge on the electrode, and the electrostatic potential at the surface of the electrode) [11]. They were able to map the theoretically most efficient heat engine, the so-called Carnot engine, onto blue engines, giving the

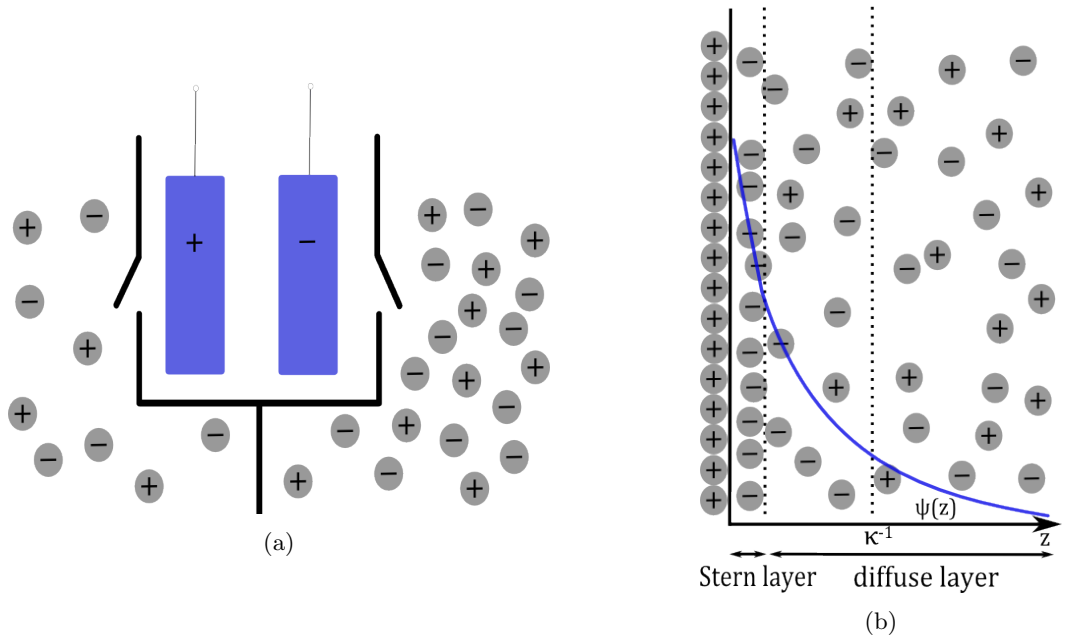

(a) (b)

Figure 1: (a) A typical setup for a blue engine using capacitive mixing. The system, consisting of two porous carbon electrodes in a volume filled with water, is connected to a reservoir with a low ion concentration (fresh water) on the left, and a reservoir with a high ion concentration (saline water) on the right. During the process, the electrodes are alternatingly charged and discharged, connected to alternatingly the fresh water reservoir or the saline water reservoir, or disconnected from both. (b) Whenever a charged object is placed into an ionic solution, an electric double-layer forms. The ions in the water try to screen the charge of the immersed object, such that the whole becomes electrically neutral. A first layer of charge stems from the immersed object, whereas a second much more diffuse second layer consists of the screening charges in the electrolyte. This screening layer can be divided in a Stern layer with a thickness of the radius of an ion, where the ions cannot be due to their finite size, and a diffuse layer. The screening typically happens within a few Debye lengths κ^{-1}, which can be found in Eq. (1). In the Stern layer, the electrostatic potential $\Psi(z)$ decreases linearly, and declines exponentially in the diffuse layer.

theoretically most efficient blue engine. From now on, this type of cycle will be referred to as the Boon cycle.

The Boon cycle is shown in Fig. 2a, where the potential Ψ of the capacitor is plotted as a function of the surface charge density σ. The system starts in point A, representing a low-charge state in saline water. The system is connected to a saline water reservoir (e.g. the sea), and in the step AB the electrodes are grand-canonically charged, very similar to the charging step in the Brogioli cycle. However, in point B the engine is disconnected from the salt water bath, and the capacitor is charged canonically, i.e. such that the number of ions in the system is fixed, during step BC. This causes the ion concentration to drop and the potential to rise, until the water salinity in the engine is equal to fresh water salinity in point C. There, the engine is connected to a fresh water reservoir (e.g. a river), and is discharged grand-canonically. In point D, the engine is disconnected from the bath, and the electrodes are discharged canonically during the DA trajectory, so that the ion concentration increases again, and the potential decreases. In point A, the water in the engine is now salty again, such that the system is left in its initial state, and the cycle can be repeated.

1.2 Electric double-layers

When a charged particle or charged electrode is placed into an ionic solution, in order to screen the charge of the object the density of oppositely charged ions near the object increases and like charges are repelled, as can be seen in Fig. 1b. Ions of like charge as the immersed object are called coions. Ions of opposite charge are referred to as counterions.

In 1879, Hermann von Helmholtz proposed the first model to treat this type of system [12]. He coined the term "electric double-layer", which consists of the combination of the layer of charge of the immersed object, and the screening layer of oppositely charged ions in the solvent. In this model, the object layer is directly screened at a distance d from the plane by a layer of counterions of diameter $\frac{d}{2}$. Beyond this

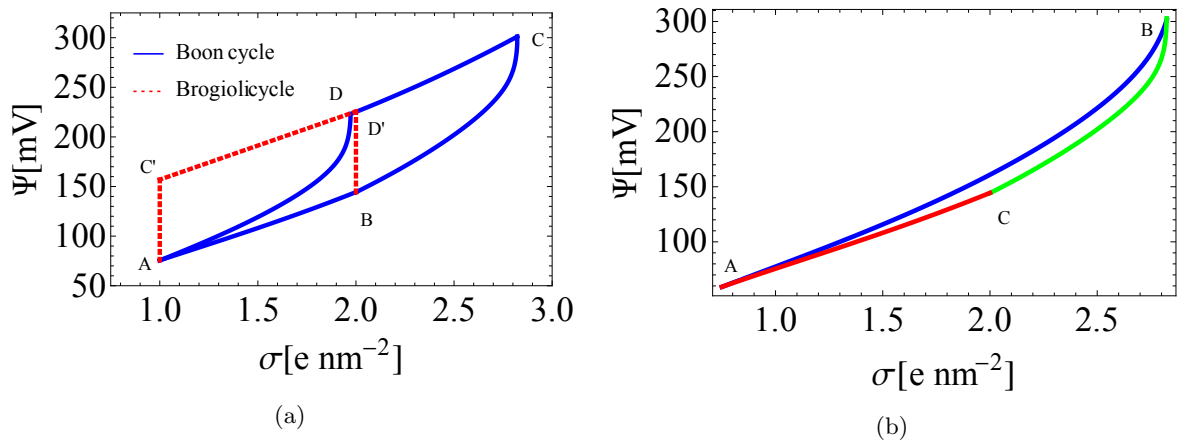

Figure 2: (a) Two charging and discharging cycles in the charge-voltage representation, for a planar capacitor with pore size $L = 4$ nm at $T = 290$ K. The red dotted ABC'D'A cycle and blue ABCDA cycle refer to the cycles decribed by Brogioli [9] and Boon [10], respectively. During step AB, the engine is connected to a salty water reservoir of high ion concentration $\rho_H = 0.6$ M. In the CD and C'D' trajectories, the engine is connected to a fresh water reservoir of low ion concentration $\rho_L = 0.024$ M. Whereas the Brogioli cycle uses a flushing step in BC' and C'A by replacing the saline water with fresh water and vice versa, in the Boon cycle the electrodes are being charged and discharged further, being disconnected from the reservoirs. The enclosed area of the cycles in this figure equals, up to a constant, the energy that can be harvested from one cycle, as will be shown in Eq.(21). The curves have been calculated numerically as described in section 3. (b) A charging and discharging cycle ABCA in the charge-voltage representation, for a planar capacitor with pore size $L = 4$ nm at $T = 290$ K. The high ion concentration in the salt water reservoir is $\rho_H = 0.6$ M, while the low fresh water ion density ρ_L equals 0.024 M. In the charging step AB, the engine of volume V_e is connected to a bath of finite size $V_b = 0.75V_e$. During this cycle, work is required to be done on the system such that the initially salt water in volume V_b is made fresh. Up to a constant, this work equals the enclosed area of the curve in this figure, as will be shown in Eq.(21). This curve has been calculated numerically, as described in section 3.

distance, coion and counterion densities equal the bulk ion density. A much more sophisticated model was introduced in 1913 by Louis Georges Gouy [13] and David Chapman [14]. Still treating the ions as pointlike particles, they modelled the counterion layer to be much more diffuse than the single plane-like Helmholtz layer. This *diffuse* double-layer is described by Boltzmann-like profiles for the ion densities $\rho_\pm(z) = \rho_s \exp(\mp \frac{e\psi(z)}{k_B T})$, with $\rho_\pm(z)$ the ion densities of positive and negative charge, ρ_s the ion density in the bulk, $\psi(z)$ the electrostatic potential, and z the distance from the electrode. Though this model already forms a much more accurate description, the assumption of the ions being pointlike is not always justified. As can be expected, this approach starts breaking down for high packing fractions, typically occurring close to the plates at high voltages. Since an infinite amount of point particles can be packed here, the capacitance in the Gouy-Chapman model shows unphysical divergence in this regime, as will be shown in Fig. 5a. In 1924, Otto Stern (also known for the Stern-Gerlach experiment) suggested a combination of the Helmholtz and the Gouy-Chapman model [15]. In reality, ions do have a finite size, and hence cannot approach the surface closer than a few ångström. The ions in the Gouy-Chapman model can only be as close to the plates as some distance d, which is taken to be the radius of the ion. Then, a Helmholtz-type layer can be found at this distance, and beyond lies the diffuse part of the double-layer. This approach is called the Gouy-Chapman-Stern model.

1.3 The reverse cycle: desalination

Whereas a blue engine produces energy by effectively making the salty water more fresh and the fresh water saltier, it is the purpose of desalination to make salt water fresh, requiring work to be done on the system. Desalination is basically the reversed process of harvesting blue energy. Continuing the analogy between heat and blue engines, a desalination device based on this scheme could be named as well a "blue fridge".

The system of interest in this thesis consists of an engine of volume V_e, with two electrodes immersed in an aqueous solution, connected to an infinitely large reservoir of salt water (like the sea) at high concentration ρ_H, and to a finite volume V_b. This latter volume is in each cycle initially filled with sea water, to be made fresh (at low concentration ρ_L) by the "fridge" during one cycle. In this system, there

is no more an infinite large fresh water reservoir, such that one of the grand-canonical steps does not take place in the desalination cycle.

The reverse process of a desalination cycle is a blue engine with limited fresh water supply [10]. If both cycles are represented in the (σ,Ψ)-plane, the only difference between them is the direction in which the trajectories are covered.

The functioning of the desalination engine can be described by a three-stage cycle ABCA as shown in Fig. 2b. In the first step AB, the engine is coupled to the volume V_b, and is initially filled with sea water. The electrodes are immersed in salt water at concentration ρ_H, and canonically charged from state A at a charge density σ_A to a higher σ_B in state B, hereby causing the salt concentration to drop to ρ_L in both V_b and V_e. Subsequently, in point B the engine and the bath are disconnected, such that the obtained fresh water in volume V_b can be secured. During the step BC the electrodes in V_e are canonically discharged to a charge density σ_C in state C, such that the ion concentration in the middle of the pores increases to the original sea-level ρ_H. Finally, the engine is connected to the salt water reservoir in state C. The trajectory CA describes the grand-canonically discharging of the system to the initial electrode charge density, where the water is salty again. Since the salt water bath is infinitely large, the transfer of a finite number of ions will not affect the bulk salt concentration in the reservoir. This means the system is back in its initial state after performing one cycle. The secured fresh water can be taken away from the volume V_b. After V_b has been filled again with sea water, the cycle can be started again.

2 Theory

2.1 Debye length and Bjerrum length

The typical distance over which the charge of an object immersed in an aqueous solution is screened, serves as a measure of the width of the electric double-layer. This measure is called the Debye length κ^{-1}, and is defined as:

$$\kappa^{-1} = \sqrt{8\pi\lambda_{\mathrm{B}}\rho_s}^{-1}, \tag{1}$$

with ρ_s being the ion density of coions and counterions in the bulk, such that the total ion bulk concentration equals $2\rho_s$. Here, λ_{B} denotes the Bjerrum length, which is defined as

$$\lambda_{\mathrm{B}} = \frac{e^2}{4\pi\varepsilon_0\varepsilon k_{\mathrm{B}}T}, \tag{2}$$

with $e = 1.602 \cdot 10^{-19}$C the elementary charge, $k_{\mathrm{B}} = 1.381 \cdot 10^{-23}$ J/K the Boltzmann constant, T the temperature in Kelvin, $\varepsilon_0 = 8.854 \cdot 10^{-12}$ F/m the electrical permittivity in vacuum, and ε and relative electrical permittivity. The Bjerrum length is the distance between two unit charges e, for which the thermal energy $k_{\mathrm{B}}T$ equals the total strength of the Coulomb interaction potential. In water ($\varepsilon = 80$) at room temperature, λ_{B} is 0.72 nm. In Fig. 3, the Debye length and the Bjerrum length are plotted against temperature for different values of the ion bulk concentration.

2.2 Dielectric constant

Unlike its name, the dielectric constant ε is not a constant, but depends on various parameters of the system and may vary with position in the electrolyte [16,17]. In this thesis, local effects will be neglected by taking ε as a global constant. However, dependences on temperature and ion bulk density will be taken into account, using the relation between ε and temperature T and ion density ρ_s in water, as found experimentally in Ref. [18],

$$\varepsilon = \varepsilon(T)a(\rho_s), \tag{3}$$

with

$$\varepsilon(T) = 249.4 - 0.788T + 7.20 \cdot 10^{-4}T^2, \tag{4}$$

and

$$a(\rho_s) = 1.000 - 0.2551\rho_s + 5.151 \cdot 10^{-2}\rho_s^2 - 6.889 \cdot 10^{-3}\rho_s^3, \tag{5}$$

with T the temperature in Kelvin, and ρ_s the ion density in the reservoir in molarity. This simplified expression will be used in the numerical calculations of this thesis.

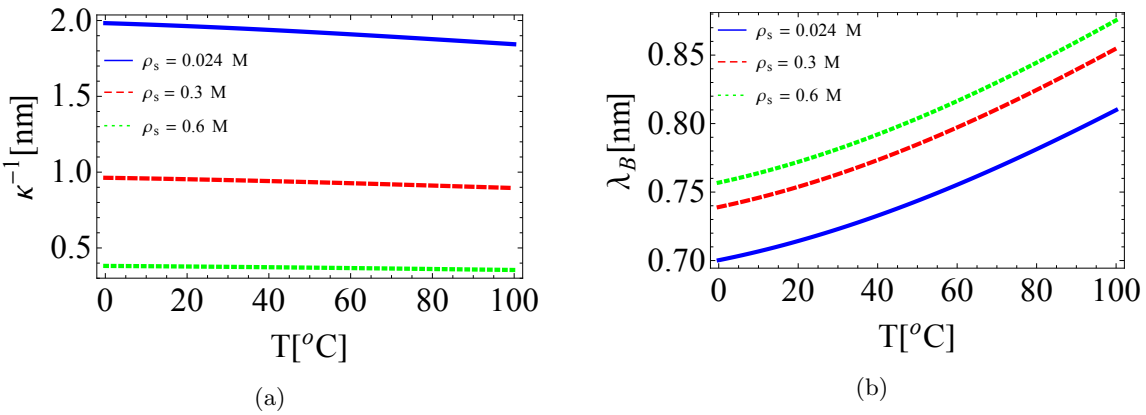

(a) (b)

Figure 3: The Debye length κ^{-1} from Eq. (1) (a) and the Bjerrum length λ_{B} from Eq. (2) (b), plotted against temperature for different ion bulk densities $\rho_s = \{0.024, 0.2, 0.6\}$ M. Regarding the dielectric constant, the temperature and ion density dependent relation (3) is used. As the temperature increases, λ_{B} rises and κ^{-1} decreases. For higher ion concentrations, λ_{B} is larger, whereas κ^{-1} is much smaller.

2.3 Poisson-Boltzmann equation

To describe an electric double-layer at an electrode, the potential and ion density profiles must be known. Since charges are present, a first ingredient for this calculation can be taken from electrostatics. The Poisson equation $\nabla^2\psi(\mathbf{r}) = -\frac{\rho(\mathbf{r})}{4\pi\varepsilon_0\varepsilon}$, with $\psi(\mathbf{r})$ the electrostatic potential and $\rho(\mathbf{r})$ the charge density at position $\mathbf{r}$, gives the relation between potential and charge at some position $\mathbf{r}$. A second equation is a mean-field Boltzmann distribution from statistical physics, where the energy of an ion with charge $\pm e$ at position z is approximated by $\pm e\psi(z)$, so that $\rho_\pm(z) = \rho_s \exp(\mp\frac{e\psi(z)}{k_\mathrm{B}T})$. The most important equation of this thesis can be obtained from these results: the Poisson-Boltzmann equation

$$\nabla^2\phi(\mathbf{r}) = \kappa^2 \sinh\phi(\mathbf{r}), \tag{6}$$

with $\phi(\mathbf{r})$ the dimensionless electric potential $\phi(\mathbf{r}) = \frac{e\psi(\mathbf{r})}{k_\mathrm{B}T}$ at position $\mathbf{r}$ outside the electrode, and κ^{-1} the Debye length, as defined in Eq. (1).

Studying blue engines implies studying electric double-layers, which involves solving the Poisson-Boltzmann equation for various systems and conditions. Together with appropriate boundary conditions, this equation can be solved analytically for some cases. Global charge neutrality of the system imposes a first boundary condition. This involves assuming the gradient of the potential goes to zero for large distances from the electrode, since any non-zero change in the first derivative implies charge being present:

$$\lim_{z\to\infty} \phi(z) = 0. \tag{7}$$

For a parallel plate capacitor with planar geometry, this condition changes to

$$\phi'(L/2) = 0, \tag{8}$$

because of charge-neutrality of a half-capacitor and the symmetry with respect to the midplane between the both plates at $z = 0$ and $z = L$.

Another condition is provided by the use of Gauss' law $\nabla \cdot E = \frac{\rho}{4\pi\varepsilon\varepsilon_0}$, where $\nabla \cdot E$ denotes the divergence of the electric field, and ρ the total electric charge density. For a one-electrode system with planar geometry, such that position $\mathbf{r}$ becomes distance z, this condition takes the form of

$$\phi'(0) = -4\pi\lambda_\mathrm{B}\sigma. \tag{9}$$

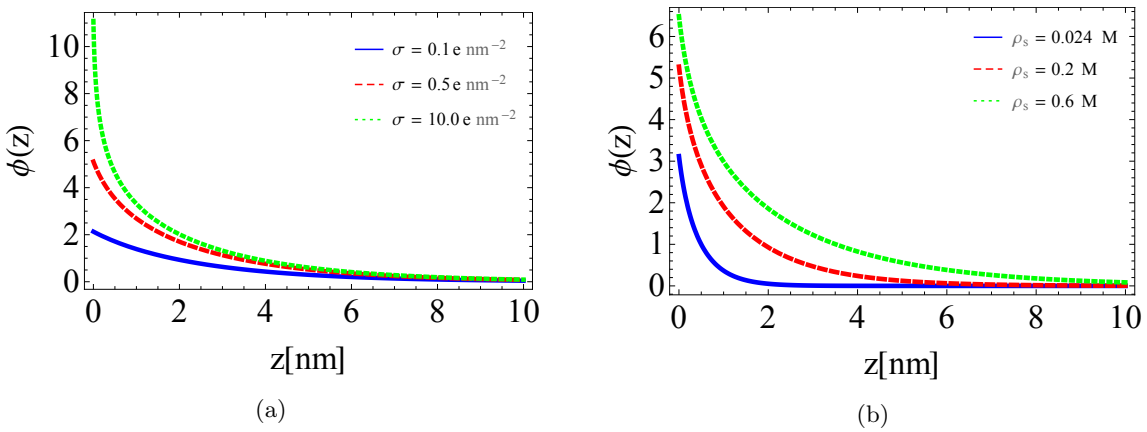

(a) (b)

Figure 4: Analytic solution to the Poisson Boltzmann equation (10) with boundary conditions Eqs. (7) and (8) for $T = 290$ K. In (a) the solution is plotted for ion bulk density $\rho_s = 0.6$ M and surface charge density $\sigma = \{0.1, 0.5, 10.0\}e$ nm^{-2}, indicated by the blue, red dashed, and green dotted lines, respectively. From Eq. (8), it can be seen that the surface charge density σ influences the steepness of the potential at the electrode. As this slope increases, the potential at the electrode rises. In (b), the solution is plotted for $\sigma = 1.0e$ nm^{-2} and $\rho_s = \{0.024, 0.2, 0.6\}$ M indicated by the blue, red dashed, and green dotted lines, respectively. As the ion bulk density ρ_s increases, the Debye length, over which the screening of the plate charges typically occurs, becomes smaller, and the electrode potential $\phi(0)$ decreases.

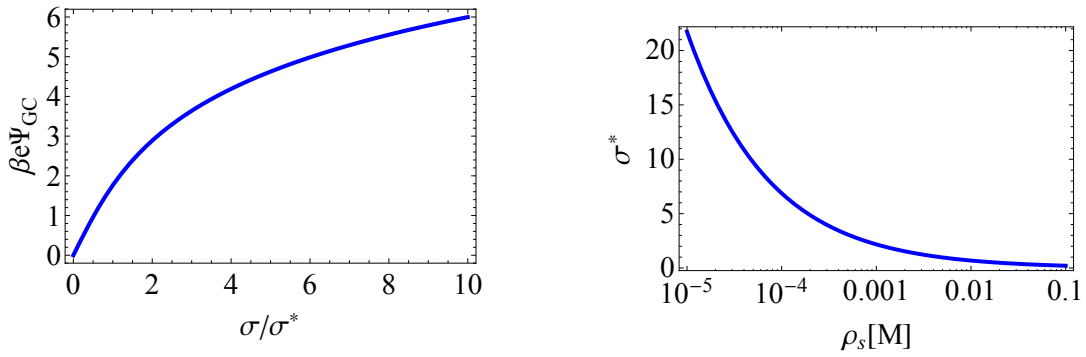

(a) (b)

Figure 5: (a) The dimensionless potential at the electrode in the Gouy-Chapman model $\beta e\Psi_{\mathrm{GC}}$ versus the dimensionless surface charge $\frac{\sigma}{\sigma^*}$, with $\beta = \frac{1}{k_{\mathrm{B}}T}$. The figure shows that for high Ψ_{GC}, the capacitance $C = \left(\frac{\mathrm{d}\Psi}{\mathrm{d}Q}\right)^{-1}$ diverges. (b) The crossover surface charge decreases when the bulk salinity ρ_s increases for $T = 290$ K. For large values of ρ_s, the linear screening regime vanishes, and ions already adsorb at the electrode for low σ.

Using boundary conditions Eqs. (7) and (9), the analytical solution to Eq. (6) for a system of one electrode of planar geometry reads

$$\phi(z) = 2\ln\left[\frac{1+\gamma\exp(-\kappa z)}{1-\gamma\exp(-\kappa z)}\right], \tag{10}$$

with integration constant $\gamma = \frac{\sqrt{1+(y/2)^2}-1}{y/2}$, where $y = \frac{4\pi\lambda_{\mathrm{B}}\sigma}{\kappa}$ is the dimensionless surface charge density. In Figs. 4a and 4b, the solution Eq. (10) is plotted for different values of surface charge density σ and ion bulk concentration ρ_s, respectively.

Since the electrodes in the engine are being charged and discharged, i.e. ions adsorb and desorb at the electrode, the cationic and anionic adsorption must be calculated. This is the excess number of ions per unit surface area, defined by

$$\Gamma(\sigma,\rho_s) = \int_{z=0}^{z=L/2} \mathrm{d}z\,(\rho_\pm(z) - \rho_s)\,. \tag{11}$$

Note that the profiles are integrated up to $z = L/2$ for the half-capacitor considered. Local charge neutrality implies that $\sigma = \Gamma_-(\sigma,\rho_s) - \Gamma_+(\sigma,\rho_s)$. The total ion adsorption is defined by

$$\Gamma_\pm(\sigma,\rho_s) = \Gamma_+(\sigma,\rho_s) + \Gamma_-(\sigma,\rho_s). \tag{12}$$

The total number of ions in the volume can thus be calculated using

$$N = 2\rho_s V + A\Gamma(\sigma,\rho_s). \tag{13}$$

Note that if the system consists of the engine only, $V = V_e$, and the relation simplifies to $N/A = \int_{z=0}^{z=L/2}\mathrm{d}z\,(\rho_+(z)+\rho_-(z))$.

Evaluating Eq. (10) at $z = 0$, the surface potential Ψ_{GC} can be derived as

$$\frac{e\Psi_{\mathrm{GC}}}{k_{\mathrm{B}}T} = 2\sinh^{-1}\left(\frac{\sigma}{\sigma^*}\right), \tag{14}$$

with $\sigma^* = \frac{\kappa}{2\pi\lambda_{\mathrm{B}}}$ the cross-over surface density that separates the linear screening regime $\sigma \ll \sigma^*$ from non-linear screening $\sigma \gg \sigma^*$. In the linear screening regime, the double layers repel coions and attract counterions at the same rate, such that the total ion concentration remains constant and the adsorption Γ is small. For higher σ, ions start being adsorbed at the electrodes. For $T = 290$ K and $\rho_s = 0.6$ M, σ^* is around $0.071e$ nm^{-2}. The behaviour of σ^* for different ρ_s can be found in Fig. 5b. Writing $Q = \sigma A$ and using Eq. (14), the differential capacitance $C = \frac{\mathrm{d}Q}{\mathrm{d}\Psi}$ can be written as

$$\frac{C_{\mathrm{GC}}}{A} = \frac{\kappa\varepsilon}{4\pi}\cosh\left(\frac{e\Psi_{\mathrm{GC}}}{2k_{\mathrm{B}}T}\right). \tag{15}$$

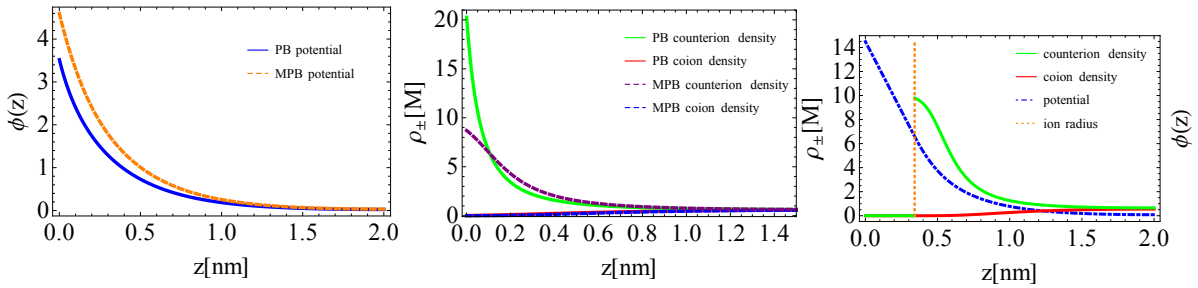

(a) (b) (c)

Figure 6: Solutions to the lattice-gas Poisson-Boltzmann equation (17) (full lines) and the normal Poisson-Boltzmann equation (6) (dashed lines) for (a) the potential and (b) the coion (red and blue) and counterion densities (green and purple). The counterion density in the lattice-gas equation is higher than in the point-particle approach, and near the plate the top of the curve is flattened, such that the unphysical steep line near the electrode of the counterion density in the Poisson-Boltzmann equation is somewhat corrected for. However, the potential profile of the lattice-gas (blue) lies much higher than that one in the normal Poisson-Boltzmann equation (orange dashed). The parameters used are $T = 290$ K, a surface charge density of $2.0e$ nm^{-2}, an ion radius of 0.34 nm, ion bulk concentration for both coions and counterions of 0.6 M, which correspond to a Debye length of 0.38 nm. (c) Including a Stern layer prohibits the ions to be closer to the plate than their own radius, indicated by the vertical orange dotted line at $r = 0.34$ nm. This can be clearly seen in the coion and counterion density profiles (increasing and decreasing full lines, respectively). The potential (blue dashed line) first decreases linearly in the Stern layer, and after in the diffuse layer exponentially.

In this equation, the afore-mentioned problem of the divergence of C at high Ψ in the Gouy-Chapman model can be observed. Rewriting $C = \left(\frac{\mathrm{d}\Psi}{\mathrm{d}Q}\right)^{-1}$ gives a way to note this divergence in Fig.5a too. The slope of the mentioned curve goes to zero, such that C will blow up.

2.4 Lattice-gas Poisson-Boltzmann equation

In the previous section the limitations of the Gouy-Chapman model, and in particular of the underlying assumption that ions can be considered as point particles, have been shown. For high packing fractions, which occur close to the plates at high voltages, some adjustments have to be made. In this section, a modification on the Poisson-Boltzmann equation (6) will be discussed, by including a finite ion size.

Taking the size of the ions to be $v = a^3$, the ion packing fraction $\eta = 2v\left(\rho_+(\mathbf{r}) + \rho_-(\mathbf{r})\right)$ can be defined, the factor 2 originating from the fact that the electrolyte contains both coions and counterions. Different routes lead to a new expression for the ionic density $\rho_\pm$. Examples include a derivation from the Helmholtz free energy of the system as done in Ref. [19], and formulating the grand-potential of the system as a functional, and next taking the derivative with respect to $\rho_\pm(\mathbf{r})$, as can be found in Ref. [10]. The ion densities can then be written as

$$\rho_\pm(\mathbf{r}) = \rho_s \frac{\exp\left(\mp\frac{e\Psi(\mathbf{r})}{k_\mathrm{B}T}\right)}{1-\eta_0+\eta_0\cosh\left(\frac{e\Psi(\mathbf{r})}{k_\mathrm{B}T}\right)}, \tag{16}$$

where $\eta_0 = 2v\rho_s$ denotes the packing fraction in the reservoir. Combining this with the Poisson equation from electrostatics, yields

$$\phi''(z) = \frac{\kappa^2 \sinh\phi(z)}{1-\eta_0+\eta_0\cosh\phi(z)}, \tag{17}$$

which will be referred to from now on as the modified or lattice-gas Poisson-Boltzmann equation. Note that for $a \to 0$ and $\eta_0 \to 0$ since $v = a^3$, this expression indeed reduces to the Poisson Boltzmann equation (6). In Figs. 6a and 6b, the normal and the lattice-gas Poisson-Boltzmann equations are compared by using their numerical solutions.

Considering the capacitance of these electric double-layers, Kornyshev was able to derive analytically a result that will be reproduced here [19]. Integrating Eq. (17) with respect to z yields

$$\phi'(z) = \mp\frac{1}{\lambda_\mathrm{B}}\sqrt{\frac{2}{\eta_0}}\sqrt{\ln\left(1-\eta_0+\eta_0\cosh\phi(z)\right)}. \tag{18}$$

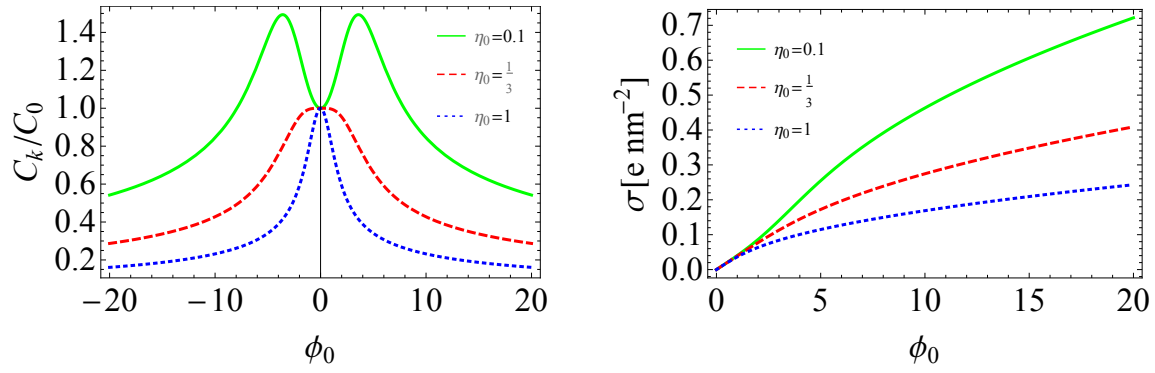

(a) (b)

Figure 7: The capacitance formula (19) as derived in Ref. [19] divided by $C_0 = \varepsilon_0\varepsilon\kappa$, plotted versus the dimensionless surface potential ϕ_0 in (a), and the surface charge density formula (20), plotted versus the dimensionless surface potential ϕ_0 in (b), for ion reservoir packing fractions $\eta_0 = \{0.1, 0.33, 1.0\}$, indicated by the green, red dashed, and blue dotted lines, respectively. For both plots, $T = 290$ K and $\rho_s = 0.6$ M. From (a) can be seen that the capacitance curve shows bell-shape behaviour for $\eta_0 > \frac{1}{3}$, camel-shape behaviour for $\eta_0 < \frac{1}{3}$, and a transition between those regimes at $\gamma = \frac{1}{3}$. From (b) can be observed that for increasing surface potentials, the surface charge density rises more strongly for lower ion packing fractions. For both figures, the parameters used are $T = 290$ K, $\rho_s = 0.6$ M, and an ion radius of 0.34 nm.

Using Gauss' law, the capacitance formula as described in Ref. [19] can be found:

$$C_{\mathrm{K}} = \varepsilon_0\varepsilon\kappa \frac{\cosh(\phi_0/2)}{1-\eta_0+\eta_0\cosh\phi_0}\sqrt{\frac{2\eta_0\sinh^2(\phi_0/2)}{\ln(1-\eta_0+\eta_0\cosh\phi_0)}}, \tag{19}$$

where $\phi_0 = \phi(z=0)$ denotes the dimensionless surface potential. Note that for $\eta_0 \to 0$, this expression reduces to the Gouy-Chapman capacitance in Eq. (15). In Fig. 7a, C_{K}/C_0 is plotted as a function of ϕ_0 for as a variety of η_0, where $C_0 = \varepsilon_0\varepsilon\kappa$.

From Eq. (18), the surface charge density σ can be rewritten in terms of the dimensionless potential $\phi(z)$,

$$\sigma = \frac{\kappa}{2\pi\lambda_{\mathrm{B}}\sqrt{2\eta_0}}\sqrt{\ln(1-\eta_0+\eta_0\cosh\phi_0(z))}. \tag{20}$$

This relation between σ and ϕ_0 is plotted in Fig.7b for different values of the ion packing fraction in the bulk η_0. It is observed that the surface density rises more strongly for lowing ion bulk packing fractions. Note that this expression reduces to Eq. (14) for small values of the dimensionless surface potential ϕ_0.

2.5 Work per cycle

As known from thermodynamics, the electrostatic work needed or extracted from one cycle equals the enclosed area in the (Q, Ψ)-plane, and can be calculated as

$$W = -\oint \Psi \mathrm{d}Q. \tag{21}$$

In this thesis, the work needed for desalination cycles at different temperature will be calculated, by first calculating numerically the curves (a typical desalination curve is shown in Fig. 2b). Once the profile of a curve is known, the work can be found by calculating its enclosed area.

3 Numerical results

3.1 Introduction

Blue engines consist of porous electrodes immersed in the electrolyte. These porous media have a highly irregular geometry on the microscale. For the model used, a crude approximation is made by assuming that geometry effects are of subordinate importance, and that the internal surface A of the electrode is primarily important to the effectiveness of blue engines. The porous electrode is simplified to a model of parallel plate capacitors, each with surface A. For the description of blue engines in this thesis, only one electrode from the capacitor is considered, without loss of generality because of the symmetry of this model. Thus, the volume of the engine can be written as $V_e = AL_e/2$, with $L_e/2$ the length of the half-capacitor. Further studies could examine the same problem in e.g. cylindrical geometries.

In order to find the optimal cycle, the parameter space of two variables is explored: the temperature T, and the ratio $x \equiv \frac{V_e}{V_b}$ between the engine volume V_e and the fresh water volume V_b that is produced over one cycle.

The central point of the calculations is the numerical solution of Eq. (17) with boundary conditions Eqs. (8) and (9). For the numerical method used, please see appendix A. Unfortunately, attempts to include a Stern layer in the used model have not been successful. Therefore, the ion density near the plates is described by the diffuse layer only. The interval $z \in [0, \frac{L}{2}]$ is divided into a grid of 5000 equidistant points. The ion volume is set to be $v = a^3$, with $a = 0.55$ nm. The distance between the two electrodes in the engine, the pore size L, is taken to be 4 nm. The afore-mentioned temperature-dependent $\varepsilon(T, \rho)$ from Eq. (3) is used to calculate the Bjerrum length, which is 70 nm for $T = 290$ K and $\rho_s = 0.6$ M. The low and high ion concentrations in the reservoir, corresponding to fresh and salty water, are taken to be $\rho_s = \rho_L = 0.024$ M and $\rho_s = \rho_H = 0.6$ M, respectively.[1]

The desalination cycle is fully characterized by the value of the surface charge in state point A ($\sigma_A = 0.75e$ nm^2), and the salinities in sea ρ_H and river ρ_L. State point B can be found using the fact that the pores have then taken up $2(\rho_H - \rho_L)(V_e + V_b)$ ions with respect to state point A. During the canonical discharging step BC, $2(\rho_H - \rho_L)V_e$ ions are dissolved in the engine, such that the salinity in the engine equals the sea salinity ρ_H again. The remaining surplus of ions $2(\rho_H - \rho_L)V_b$ determines the value of σ_C, and this amount is released into the salt water bath during the grand-canonical discharging trajectory CA.

In this system, there is a very clear physical boundary. The potential Ψ must not be larger than $\Psi_{max} = 1.229$V, which corresponds to a dimensionless potential $\phi_{max} \simeq 50$ [20].[2] If the potential is increased beyond this value, a reduction-oxidation reaction may happen in the form of electrolysis, hence removing our electrolyte. Therefore, values of the surface charge density σ larger than, say, $5e$ nm^{-2}, should be avoided.

3.2 Investigating the desalination cycle

A first step consists of investigating the influence of the temperature and ion density dependent dielectric constant $\varepsilon(T, \rho_s)$. Fig. 8 shows the desalination curve from Ref. [10] where $\varepsilon = 80$, compared to a curve where the experimental dielectric constant from Eq. (3) is taken into account, i.e. a varying the dielectric constant, since ρ_s varies throughout the cycle. For $T = 290$ K, $\varepsilon(\rho_s = 0.024) = 74.9$, and $\varepsilon(\rho_s = 0.6) = 80.9$, showing a difference of 8% for the extremes in ion bulk concentration used. The desalination cycle with a fixed $\varepsilon = 80$ requires an energy input of $W/V_b = 2.56$ kJ per secured liter of fresh water, or $W/A = 0.962$ k$_\mathrm{B}$T nm^{-2}. Using Eq. (3), this becomes $W/V_b = 1.84$ kJ per secured liter of fresh water, or $W/A = 0.691$ k$_\mathrm{B}$T nm^{-2}. Clearly, taking a fixed $\varepsilon = 80$ leads to an overestimation of the work required per cycle. A second point of interest are the potential profiles and ion density profiles at the three state points A, B, and C of the desalination cycle, shown in Fig. 9.

[1] Note that one can easily convert concentrations between molarity and nm^{-3} by using the Avogadro constant $N_\mathrm{A} = 6.022 \cdot 10^{23}$ mol^{-1}.

[2] This value is the standard reduction potential (i.e. at temperature $T = 298$ K, and pressure $p = 1$ atm, equivalent to $p = 101.325$kPa) for which the chemical reaction $O_2 + 4H^+ + 4e^- \rightleftharpoons 2H_2O$ takes place. Reduction potentials at other temperatures can be calculated as described in Ref. [21]. However, since this thesis is not written for experimental purposes, calculating reduction potentials for different circumstances goes beyond its scope. Therefore, the standard potential is taken into account as a fixed physical constraint in the numerical calculations.

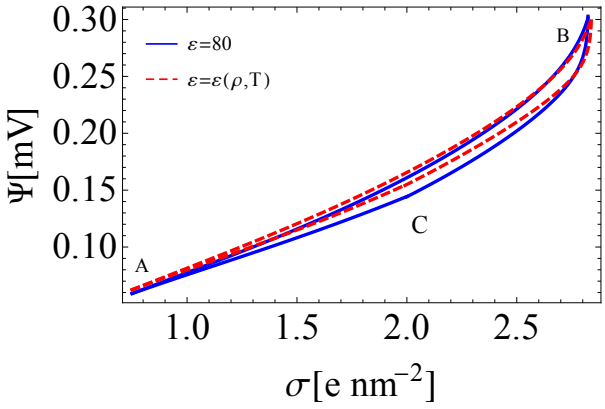

Figure 8: Desalination cycles ABCA with $\varepsilon = 80$ (full blue curve), and $\varepsilon = \varepsilon(T, \rho)$ (dashed red curve) from Eq. (3). For both cycles, the same parameters have been used: $T = 290$ K, $x = 1.33$, and the width of the half-capacitor $L = 2$ nm. The cycle with a fixed $\varepsilon = 80$ yields a required energy input of $W/V_b = 2.56$ kJ per secured liter of fresh water, or $W/A = 0.962$ k_BT nm^{-2}. Using Eq. (3), this becomes $W/V_b = 1.84$ kJ per secured liter of fresh water, or $W/A = 0.691$ k_BT nm^{-2}. Taking a fixed $\varepsilon = 80$ clearly leads to an overestimation of the work required per cycle.

3.3 Temperature effects

For increasing temperatures, the Debye length κ^{-1} from Eq. (1) decreases, resulting in a shorter distance in which the surface charges on the plate are screened. Since the electrolyte is an aqueous solution, the natural range in which the temperature can be varied is between $T = 0\,^\circ$C or $T = 273$ K, and $T = 100\,^\circ$C or $T = 373$ K. In the calculations, a step size of $10\,^\circ$C has been used on this interval, such that for 11 different temperatures the required work per cycle is calculated. This has been done for two different values of the volume ratio x, being $x = 1.33$ and $x = 5.0$.

Fig. 10 represents the results of the calculations. Figs. 10a and 10c show desalination cycles for different temperatures in the (σ,Ψ)-representation, x being 1.33 and 5.0, respectively. As the temperature increases, the surface potential at the electrode for which the cycle takes place also becomes larger. The work required for one cycle was calculated using Eq. (21). For the parameters of the cycle discussed here, at a temperature of $T = 273$ K, a value of $W/V_b = 1.74$ kJ per secured liter of fresh water, or $W/A = 0.695$ k_BT nm^{-2}, was found for $x = 1.33$. For $x = 5.0$, a value of $W/V_b = 2.01$ kJ per secured liter of fresh water, or $W/A = 0.214$ k_BT nm^{-2} is reported in this thesis. As the temperature rises, the work required to perform one cycle also increases. Figs. 10b and 10d show the calculated work for different temperatures, normalized to the cost per cycle W_{273K} at $T = 273$ K. For $x = 1.33$, this yields the fitted linearly relation

$$\frac{W(T)}{W_{273K}} = 1.00312 + 0.00309T. \tag{22}$$

This relation implies an increase in work of 0.31% per degree. This leads up to a difference of 30.9% at the highest temperature if the extremes are compared. Regarding $x = 5.0$, the normalized work curve is fitted linearly with the relation

$$\frac{W(T)}{W_{273K}} = 1.00183 + 0.00345T, \tag{23}$$

implying an increase in work of 0.35% per degree, and leading up to a maximal difference of 34.5% if the extremes are compared.

These results imply that desalination processes are the most efficient, i.e. cost the least amount of work, at very low temperatures, say in the Arctic regions.[3]

The same results as in Fig. 10b have been found by others, using the same type of model, and a hard-sphere model described by Fundamental Measure Density Functional Theory. [4]

[3] This means, however, for the reverse process (a blue engine with a limited fresh water supply), that the energy gained by the capacitive mixing of salt and fresh water at a given temperature is optimal at high temperatures, say in the tropics.

[4] M. Janssen and A. Härtel, work in progress.

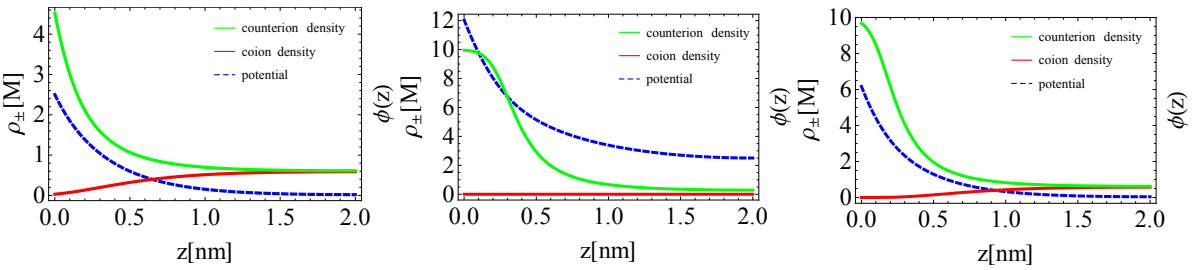

Figure 9: Potential profiles (dashed lines) and co- and counterion density profiles (increasing and decreasing, respectively, full lines) in the three states (a) A, (b) B, and (c) C of the desalination cycle as described in Fig.2b and Fig.8 (dashed curve). For this cycle, $T = 290$ K, half-capacitor width $L = 2$ nm, an ion radius of 0.34 nm, and volume ratio $x = 1.33$. The surface charge density in state point A is fixed at $\sigma_A = 0.75e$ nm^{-2}. Together with the fresh water reservoir salinity $\rho_s = 0.024$ M (in point B) and saline water ion concentration $\rho_s = 0.6$ M (in points A and C), this determines the values of the surface charge density in state points B and C, with $\sigma_B = 2.84e$ nm^{-2} and $\sigma_C = 1.99e$ nm^{-2}. As the Debye length depends on salinity, this length is $\kappa^{-1} = 0.38$ nm for $\rho_s = 0.6$ M in A and C , and $\kappa^{-1} = 1.97$ nm for $\rho_s = 0.024$ M in B. It can be seen that the ion density flattens near the electrode, and unphysical high ion packings are prevented. The fact that the potential is much higher for electrolyte with a low ion concentration than with a high ion concentration can be seen clearly from the comparison of on the one hand state point B at $\rho_s = 0.024$ M, and on the other hand the state points A and C at $\rho_s = 0.6$ M.

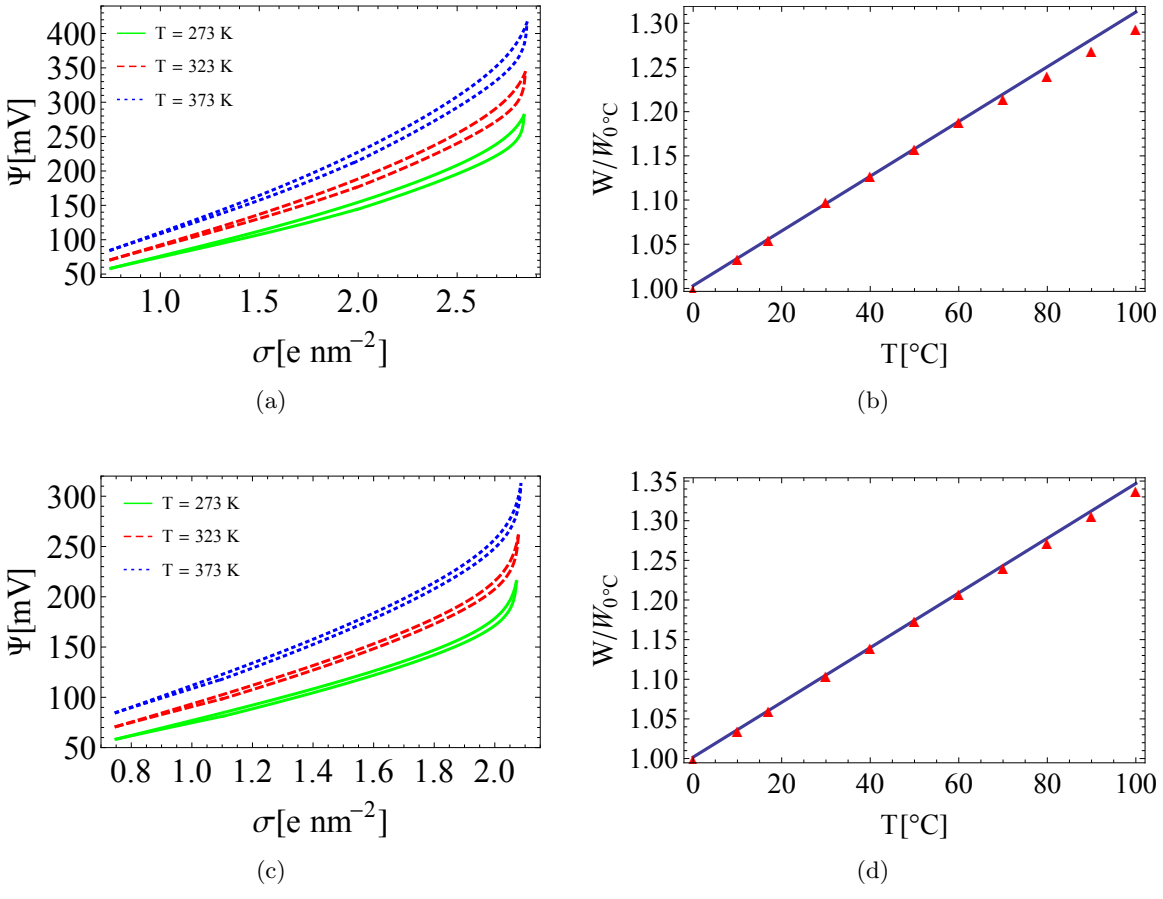

Figure 10: On the left, desalination cycles are shown for different temperatures for $x = 1.33$ (a) and for $x = 5.0$ (c). It can be seen that as the temperature increases, the surface potential at the electrode for which the cycle takes place also increases. The figures on the right represent the calculated work for different temperatures, normalized to the cost per cycle W_{273K} at $T = 273$ K for $x = 1.33$ (b) and for $x = 5.0$ (d). Clearly, as temperature increases, the amount of needed work also increases. An increase of 0.31% and 0.35% per degree of temperature increase is observed for $x = 1.33$ and for $x = 5.0$, respectively. Thus, the desalination cycle is optimal for low temperatures. These figures represent the results of numerical calculations.

The comparison of the calculations for both $x = 1.33$ and $x = 5.0$ already shows a significant difference between required work per secured liter of fresh water for different amounts of secured fresh water during one cycle. This parameter space will be explored further in the next section.

3.4 Effects of the volume ratio between the engine and the fresh water volume

In order to study the effect of the size of the fresh water volume V_b coupled to the engine of size V_e in the AB trajectory, it is useful to consider the ratio x. This ratio influences the cycle in two closely related ways. First, the behaviour of the AB curve, during which the engine is connected to the bath, is determined by x. For small bath volumes compared to the engine volume and thus large x, this step becomes essentially canonical and will resemble the BC curve, where the system is canonically discharged. As x decreases, the engine is coupled to an increasingly reservoir-like volume. The charging curve will become more grand-canonical, and will start resembling the grand-canonical discharging trajectory CA. Note that for a real thermodynamically large bath, the uptake of ions by the electrodes does not influence the reservoir ion density ρ_s, whereas the trajectory consists of decreasing the ion density in the engine from sea to river salinity. The second way how the cycle is influenced by x, is that it determines the value of σ_C, the surface charge density in state point C. The number of ions originating from the bath that is adsorped on the electrodes during the AB stage, must be desorbed while the system is in contact with the salty water reservoir. The ratio x, or the relative number of ions from the bath, therefore determines the length of the grand-canonical discharging step CA. Since σ_A is fixed, this influences the value of σ_C. Note that this change also stems from the increasingly reservoir-like character of the fresh water volume for smaller x. In Fig. 11 desalination cycles are plotted for $x = 1.0$, $x = 2.5$, and $x = 10.0$. It can be seen that for increasing x the canonical charging AB curve starts resembling the canonical discharging BC trajectory, as a declining number of ions stemming from the fresh water volume must be dumped in the salty water reservoir. Numerical calculations have been performed in the range between $x = 0.5$ and $x = 10$. The same parameters from the previous section are used, with the only difference that the system operates at constant temperature $T = 290$ K. From Fig. 12a, it can be observed that for increasing x the cycle takes place at substantial lower values for the voltage Ψ and surface density σ. The work required for one cycle was calculated using Eq. (21). As can be seen from Fig. 12a, the enclosed area decreases for higher values of x. However, the amount of secured fresh water during each cycle also diminishes. Interestingly, the amount of energy needed per liter of secured fresh water, shown in Fig. 12b, diminishes with declining x. This suggests that desalinating is optimal for small x, i.e. for large amounts of secured fresh water during one cycle.

The reverse process of desalination, i.e. a blue engine with a limited fresh water supply, is the most beneficial if the energy harvested per liter of fresh water is maximal. This is the case for small values of x. However, for small x, the bath volume is much larger than the engine volume. Consequently, the uptake of ions in the AB trajectory by the electrodes must be much larger. Since the system has a constraint on the value of Ψ in order to prevent electrolysis from happening, it must be noted that one can not exceed some minimal value for x. If this would be the case, the cycle can not be performed. However, for $x \approx 0.2$

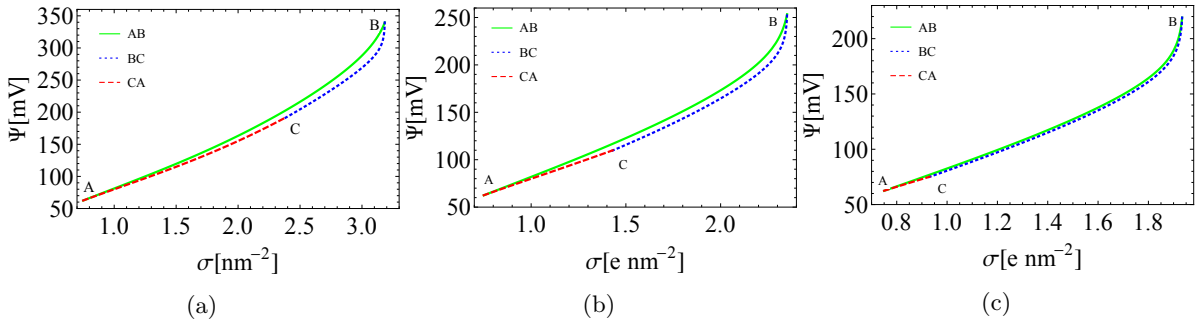

Figure 11: Desalination cycles for (a) $x = 1.0$, (b) $x = 2.5$, and (c) $x = 10.0$, x denoting the fraction between engine volume and secured fresh water volume per cycle $\frac{V_e}{V_b}$, using $T = 290$ K, a fixed $\sigma_A = 0.75e$ nm^{-2}, the salty water reservoir concentration $\rho_s = 0.6$ M, and the ion bulk density in the secured fresh water volume as $\rho_s = 0.024$ M. As x increases, the AB trajectory starts to resemble more the canonical discharging step BC. For smaller values of x, the AB curve starts to look more like the grand-canonical discharging stage CA, as more ions must be adsorped from V_b to make its water fresh and dumped later in the reservoir.

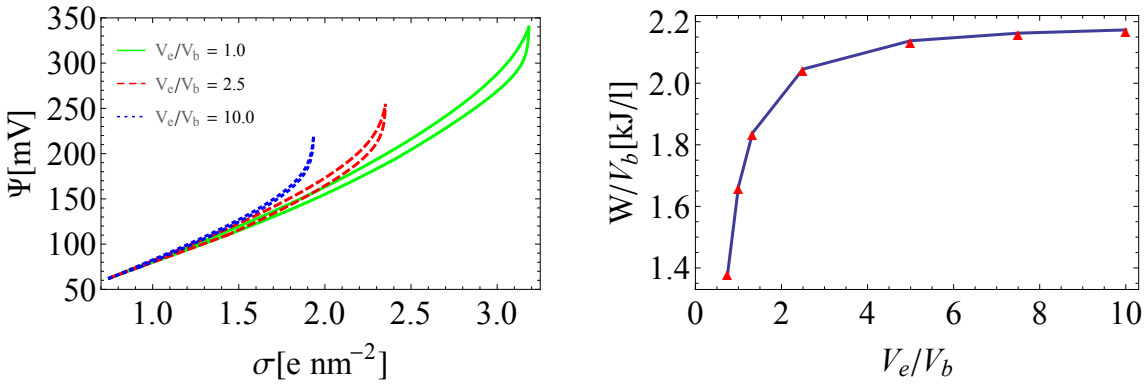

(a) (b)

Figure 12: (a) Desalination cycles for different temperatures. It can be seen that for increasing x, the values of the surface charge density and surface potential for which these cycles occur decrease. The enclosed area, and thus the work needed per cycle, also decreases. However, per cycle also a smaller amount of fresh water is secured. (b) The required work per secured liter of fresh water plotted against the volume ratio x. The work needed is obviously minimal for low values of x, i.e. large amounts of secured fresh water per cycle. These figures represent the results of numerical calculations.

state point C starts to cross the AB trajectory in the calculations. This is unphysical behaviour, since the canonical charging stage AB by definition can not be steeper than the grand-canonical discharging step CA in the charge-voltage representation. This showed a limitation in the calculations in the used model, which unfortunately could not be solved. Therefore, the possibility of calculating this minimum lies beyond the scope of the model.

4 Conclusion and outlook

In this thesis, capacitive demixing of salty water, or water desalination, is described. In a three-stage cycle a finite volume of initially saline water is made fresh, requiring work to be done on the system. The aim has been to find the optimal cycle, such that the required work per liter desalinated water is minimal. Calculations regarding temperature effects show that the difference between the work needed at 273 K and 373 K, can go up to 31% for $x = \frac{V_e}{V_b} = 1.33$, with $\frac{W}{V_b} = 1.74$ kJ per liter desalinated water at $T = 0\,^{\circ}\text{C}$. For $x = 5.0$, the difference between $0\,^{\circ}\text{C}$ and $100\,^{\circ}\text{C}$ is even 35%, with $\frac{W}{V_b} = 2.01$ kJ/liter at $T = 0\,^{\circ}\text{C}$. Desalination processes are therefore the most efficient at low temperatures. The second line of calculations focussed on the influence of the volume ratio x, and showed that the desalination cycle costs the least amount of energy per liter of secured fresh water for small x, i.e. large fresh water bath volumes compared to the engine volume. These results will help in the search for a desalination process that requires a minimum input of energy.

In fact, these results indicate too that the reversed desalination process, i.e. a blue engine with limited fresh water supply, is a very promising technology to generate sustainable energy. Since the outcome of the calculations also applies to the blue engine, it shows that there is a great energy potential that could be harvested by capacitive mixing of fresh and saline water. Thus, the largest amount of energy can be harvested from high temperature systems, and for which the volume of mixed fresh water per cycle is small compared to the engine volume. Assuming that the engine described in this thesis could harvest the energy from the complete outflow of the Rhine, this would result in an energy production of $9.52 \cdot 10^7$ kWh a day, equivalent to 2.95% of the national energy consumption of the Netherlands. These numbers are of course rough estimates, but do give an idea of the vast potential this capacitive mixing technology offers.[5]

Improvements on the current work include implementing a Stern layer in the model, and taking into account a more sophisticated description of the dielectric constant. Furthermore, the calculated work needed for desalination cycles for different temperatures has been fitted linearly. More calculations could increase the accuracy of the fit. The distance between the two plates of the capacitor, taken constant throughout this work, gives another parameter space that could be explored. Additionally, as the electrodes in a blue engine are made of porous carbon and the pore size will vary throughout the electrode, a pore size distribution could be taken into account. Also, capacitors with different geometries could be studied. Another interesting line of work is investigating the work input per time, or the power needed to perform a cycle. This will prove if the described processes are truly efficient in time, which is of great importance for this technique to eventually become a useful application in society.

[5] The outflow of the Rhine is about 2200 m^3/s. If one supposes that a blue engine behaves fully according to the model used in this thesis and an engine efficiency of 100%, an energy output of 1.80 kJ/liter fresh water at $T = 283$ K and $x = 1.33$, would lead to $9.52 \cdot 10^7$ kWh a day. The national energy consumption of the Netherlands is roughly 193 kWh per person per day, such that the harvested energy is 2.95% of the national energy consumption. Please note that these numbers are very rough estimates, and their only purpose is to give an idea of the order of magnitude of energy that this capacitive mixing technology offers.

5 Acknowledgements

First of all, I would like to thank my supervisors René, Andreas and Mathijs, who have put many hours in guiding Sander and me during this bachelor's research project, and from whom I have learned a lot. It has been a great pleasure finding their doors always open for questions and help. Also thanks to Sander, my partner in this "blue energy"-crime, with whom I have spent many hours reading, programming, writing, and discussing the numerous problems we faced on the way.

References

[1] Hamelers, H. V. M., Schaetzle, O., Paz-Garca, J. M., Biesheuvel, P. M., & Buisman, C. J. N. (2013). Harvesting energy from CO2 emissions. Environmental Science & Technology Letters.

[2] Rahman, M., Paul, N., Islam, M. S., & Rashed, M. S. (2013). Power Generation from Sea Wave: An Approach to Create Renewable Energy. Global Journal of Researches In Engineering, **13**(1).

[3] Castellucci, V., Waters, R., Eriksson, M., & Leijon, M. (2013). Tidal effect compensation system for point absorbing wave energy converters. Renewable energy, **51**, 247-254.

[4] Pattle, R. E. (1954). Production of Electric Power by mixing Fresh and Salt Water in the Hydroelectric Pile. Nature, **174**.

[5] Levenspiel, O., & de Nevers, N. (1974). The Osmotic Pump. Science, **183**(4121), 157-160.

[6] Post, J. W., Veerman, J., Hamelers, H. V., Euverink, G. J., Metz, S. J., Nymeijer, K., & Buisman, C. J. (2007). Salinity-gradient power: Evaluation of pressure-retarded osmosis and reverse electrodialysis. Journal of Membrane Science, **288**(1), 218-230.

[7] Weinstein, J. N., & Leitz, F. B. (1976). Electric power from differences in salinity: the dialytic battery. Science, **191**(4227), 557-559.

[8] Post, J. W., Veerman, J., Hamelers, H. V., Euverink, G. J., Metz, S. J., Nymeijer, K., & Buisman, C. J. (2007). Salinity-gradient power: Evaluation of pressure-retarded osmosis and reverse electrodialysis. Journal of Membrane Science, **288**(1), 218-230.

[9] Brogioli, D. (2009). Extracting renewable energy from a salinity difference using a capacitor. Physical review letters, **103**(5), 058501.

[10] Boon, N., & van Roij, R. (2011). Blue energy from ion adsorption and electrode charging in sea and river water. Molecular Physics, **109**(7-10), 1229-1241.

[11] van Roij, R. (2012). Statistical thermodynamics of supercapacitors and blue engines. arXiv preprint arXiv:1211.1269.

[12] Helmholtz, H. V. (1879). Studien über electrische Grenzschichten. Annalen der Physik, **243**(7), 337-382.

[13] Gouy, M. (1910). Sur la constitution de la charge electrique a la surface d'un electrolyte. J. Phys. Theor. Appl., **9**(1), 457-468.

[14] Chapman, D. L. (1913). LI. A contribution to the theory of electrocapillarity. The London, Edinburgh, and Dublin Philosophical Magazine and Journal of Science, **25**(148), 475-481.

[15] Stern, O. (1924). The theory of the electrolytic double-layer. Zeit. Elektrochem, **30**, 508-516.

[16] Ben-Yaakov, D., Andelman, D., Harries, D., & Podgornik, R. (2009). Beyond standard Poisson-Boltzmann theory: ion-specific interactions in aqueous solutions. Journal of Physics: Condensed Matter, **21**(42), 424106.

[17] Hatlo, M. M., van Roij, R. H. H. G., & Lue, L. (2012). The electric double layer at high surface potentials: The influence of excess ion polarizability. EPL (Europhysics Letters), **97**(2), 28010.

[18] Sambriski, E. J., Schwartz, D. C., & De Pablo, J. J. (2009). A mesoscale model of DNA and its renaturation. Biophysical journal, **96**(5), 1675-1690.

[19] Kornyshev, A. A. (2007). Double-layer in ionic liquids: paradigm change?. The Journal of Physical Chemistry B, **111**(20), 5545-5557.

[20] Handbook of Chemistry and Physics, 69th edition, eds. R.C. Weast, M.J. Astle, W.H. Beyer, CRC Press, Boca Raton (1988).

[21] Bratsch, S. G. (1989). Standard electrode potentials and temperature coefficients in water at 298.15 K. American Chemical Society and the American Institute of Physics for the National Institute of Standards and Technology.

Appendix A Numerical method

In this thesis, the so-called "shooting method" is used to solve numerically the lattice-gas Poisson-Boltzmann equation (17) for the dimensionless potential $\phi(z)$ and co- and counterion densities $\rho_{\pm}(z)$ as a function of the distance from the electrode z.

In general, next to a differential equation, two boundary conditions of the form $f(z_1) = a$ and $f(z_2) = b$ can be imposed. The shooting method searches through possible starting conditions of the form $f'(z_1) = c$, so that upon evaluating the differential equation it satisfies the two boundary conditions.

From the lattice-gas Poisson-Boltzmann equation

$$\frac{\mathrm{d}^2\phi(z)}{\mathrm{d}z^2} = \frac{\kappa^2 \sinh\phi(z)}{1-\eta_0+\eta_0\cosh\phi(z)},$$

the first derivative can be named $\frac{\mathrm{d}\phi(z)}{\mathrm{d}z} = \xi$. This results in two equations:

$$f_1(\phi, z, \xi) = \frac{\mathrm{d}\xi}{\mathrm{d}z} = \frac{\kappa^2 \sinh\phi(z)}{1-\eta_0+\eta_0\cosh\phi(z)}, \quad \text{and} \tag{24}$$

$$f_2(\phi, z, \xi) = \frac{\mathrm{d}\phi(z)}{\mathrm{d}z} = \xi. \tag{25}$$

The next step is to introduce a grid of $N+1$ points on the interval $z \in [0, L]$. The interval consists of N intervals of length $h = \frac{L}{N}$, such that $z_i = ih$ with $i = 0, 1, 2, ..., N$. The dimensionless potential $\phi(z)$ can now be discretized, such that $\phi(z_i) \equiv \phi_i$. Note that the accuracy of this method increases when using a smaller step size h. All this yields three equations:

$$z_{i+1} = z_i + h, \tag{26}$$

$$\phi_{i+1} = \phi_i + hf_1(\phi_i, z_i, \xi_i), \quad \text{and} \tag{27}$$

$$\xi_{i+1} = \xi_i + hf_2(\phi_i, z_i, \xi_i). \tag{28}$$

With these equations, the further progress of the function is calculated, and checked if it corresponds with the other two boundary conditions (this approach "shoots" and sees if the found solution fits). Based on how the found solution diverges, one can easily adjust the third imposed boundary condition, until finally an acceptable solution is found.

Note that this method also works the other way around: instead of imposing e.g. $f(z_2) = b$, one can also impose $f'(z_1) = c$. The shooting method then searches through starting conditions of the form $f(z_2) = b$, so that upon evaluating the differential equation it satisfies the two imposed boundary conditions.